Palaeogeography, Palaeoclimatology, Palaeoecology 516 (2019) 90–100

Contents lists available at ScienceDirect

Palaeogeography, Palaeoclimatology, Palaeoecology

journal homepage: www.elsevier.com/locate/palaeo

Clay mineral assemblages in the Zhaotong Basin of southwestern China: Implications for the late Miocene and Pliocene evolution of the South Asian monsoon

Pei Li[a,b], Chunxia Zhang[a,c,d,*], Zhengtang Guo[a,b,d], Chenglong Deng[e,b], Xueping Ji[f,g], Nina G. Jablonski[h], Haibin Wu[a,b,d], Rixiang Zhu[e,b]

[a] Key Laboratory of Cenozoic Geology and Environment, Institute of Geology and Geophysics, Chinese Academy of Sciences, Beijing 100029, China
[b] University of Chinese Academy of Sciences, Beijing, China
[c] College of Earth Science and Engineering, Shandong University of Science and Technology, Qingdao 266590, Shandong Province, China
[d] CAS Center for Excellence in Life and Paleoenvironment, Beijing 100044, China
[e] State Key Laboratory of Lithospheric Evolution, Institute of Geology and Geophysics, Chinese Academy of Sciences, Beijing 100029, China
[f] Department of Paleoanthropology, Yunnan Institute of Cultural Relics and Archaeology, Kunming 650118, China
[g] Joint Research Center for Human Evolution and Environmental Changes of Yunnan, Zhaotong 657000, China
[h] Department of Anthropology, The Pennsylvania State University, University Park, PA 16802, USA

ARTICLE INFO

Keywords:
Global cooling
Yunnan Province
Clay fraction
Sedimentary

ABSTRACT

The characteristics of the evolution of the South Asian monsoon during the late Miocene through the Pliocene are highly debated. To obtain a better understanding, we studied the clay mineral assemblages and the clay fraction content of a high-quality sedimentary sequence (borehole core ZK1) spanning the interval of 8.8–2.62 Ma in the Zhaotong Basin, southwestern Yunnan Province, on the southeastern margin of the Tibetan Plateau. Smectite, kaolinite, illite and vermiculite were the four main clay minerals identified, and changes in their relative abundance reveal a distinct pattern of climate change during the study interval. Until the very late Miocene kaolinite and smectite, with a small amount of illite, were dominant, suggesting a relatively warm and humid climate; from ~6.2 to ~2.8 Ma smectite was dominant, with a minor amount of kaolinite and illite, indicating a relatively cool and humid climate; and from ~2.8 to 2.62 Ma vermiculite (HIV) and illite were dominant, with a minor amount of kaolinite, indicating a relatively cold and humid climate. The variation in clay mineral assemblages indicate substantial changes in the South Asian monsoon in the Zhaotong Basin that promoted a change from a warm and humid climate in the late Micoene to cool and humid climate in the very late Miocene through Pliocene, followed by a gradual trend towards a cold and humid climate in the very late Pliocene. Comparison with records from elsewhere indicates that the observed variations in the South Asian monsoon were mainly controlled by global cooling rather than by Tibetan Plateau uplift.

1. Introduction

The period from the late Miocene to the Pliocene was characterized by dramatic global environmental changes, as demonstrated by marine oxygen and carbon isotope records that indicate significant climatic cooling, reflecting the rapid expansion of Northern Hemisphere ice-sheets (Shackleton et al., 1995; Zachos et al., 2001). In addition, the origin of the hominin lineage appears to have occurred at ~7 Ma (Brunet, 2010); there was a reorganization of the ocean-atmospheric circulation system recombination (Flower and Kennett, 1993; Ramstein et al., 1997); large-scale C_3/C_4 vegetation changes occurred in a large area of the tropics and subtropics during the late Miocene(Quade et al., 1989; Cerling et al., 1997); and significant desertification occurred in the interior of Asia during the late Miocene through Pliocene (An et al., 2001; Guo et al., 2004).

The Asian monsoon system, including the East Asian monsoon and South Asian monsoon, is a major component part of the global climate system; both are characterized by a seasonal wind reversal and precipitation changes associated with the differential heating of land and sea (Reuter et al., 2013). Numerous studies have been undertaken to reconstruct the history of the Asian monsoon system during the late Miocene through Pliocene, especially of the East Asian monsoon. Our

* Corresponding author at: Institute of Geology and Geophysics, Chinese Academy of Sciences, No. 19 Bei Tucheng Xilu, Chaoyang Dist., Beijing 100029, China.
E-mail address: cxzhang@mail.iggcas.ac.cn (C. Zhang).

https://doi.org/10.1016/j.palaeo.2018.11.039
Received 21 May 2018; Received in revised form 27 November 2018; Accepted 30 November 2018
Available online 05 December 2018
0031-0182/ © 2018 Elsevier B.V. All rights reserved.

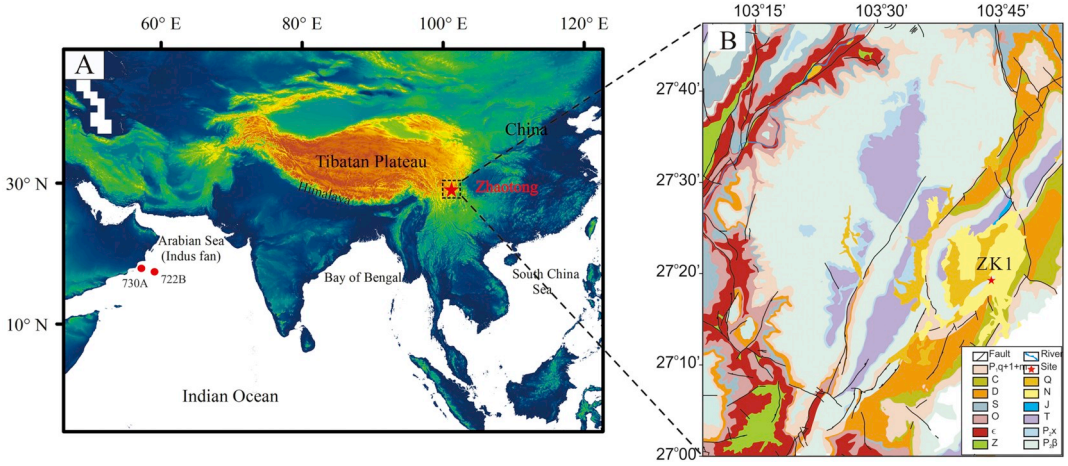

Fig. 1. A., Location of the Zhaotong site in Yunnan Province, China; B., Schematic geological map of the area surrounding borehole ZK1 in the Zhaotong Basin. Abbreviations: Z: phyllite, quartz sandstone and carbonate; ϵ: dolomite, marlite and shellstone; O: shellstone, sandstone, dolomite and limestone; S: shellstone, sandstone, siltstone and limestone; D: sandstone, shellstone, dolomite and limestone; C: limestone, sandstone and dolomite; P_1: limestone, shellstone, sandstone and dolomite; P_2: Emeishan balsalt; T: sandstone, siltstone, marlite, dolomite; J: mudstone, siltstone, sandstone and marlite; K: sandstone; N: clay, lignite and sandy conglomerate; Q: gravel, sand and clay; $P_2\chi$: conglomerate, sandstone, shale with interlayer of coal; $P_2\beta$: Emeishan balsalt with interlayer of tuff. (Modified from Zhang et al., 2016).

knowledge of the evolution of the South Asian monsoon during the late Miocene to Pliocene is based mainly on the marine record (Kroon et al., 1991; Gupta and Srinivasan, 1992; Prell and Kutzbach, 1992; Prell et al., 1993; Gupta et al., 2001; An et al., 2001; Clift et al., 2008; Patnaik et al., 2012; Tripathi et al., 2017) and on fluvial sediments of the Siwalik Group in the southern part of the Himalaya (Quade et al., 1989; Cerling et al., 1993; Quade et al., 1995; Cerling et al., 1997; Hoorn et al., 2000). Sedimentary records from the Arabian Sea and Indian Ocean indicate that the South Asian monsoon may have intensified during the late Miocene through Pliocene (Kroon et al., 1991; Prell and Kutzbach, 1992; Prell et al., 1993; An et al., 2001; Zheng et al., 2004), while some other records indicate that its intensity may have decreased during this interval (Hoorn et al., 2000; Sanyal et al., 2004, 2005; Clift et al., 2008; Tripathi et al., 2017). Thus, the evolution of the South Asian monsoon during the late Miocene to Pliocene remains controversial. To help resolve the issue, more continental sedimentary records, with a precise chronological framework, are needed from representative areas of the South Asian monsoon region.

Yunnan Province is located on the southeastern margin of the Tibetan Plateau and contains numerous sedimentary basins, making it one of the most important regions for research on the late Cenozoic climatic change. Part of Yunnan may be affected by the East Asian monsoon, but the climate of most of Yunnan is mainly controlled by the South Asian monsoon. Much research on climatic evolution during the late Cenozoic have been carried out in the various basins in Yunnan Province (e.g., Zhao et al., 2004; Xu et al., 2004; Kou et al., 2006; Xu et al., 2008; Xia et al., 2009; Jacques et al., 2011; Zhang et al., 2012; Xing et al., 2012; Su et al., 2013; Chang et al., 2015; Zhang et al., 2016). The carbon and oxygen isotopic composition of soil samples and teeth of fossil herbivores from the Yuanmou Basin indicates a climatic drying and a change from a largely densely-forested environment at ~8 Ma to a more open environment with a mosaic of forest and grassland after ~3–4 Ma (Biasatti et al., 2012). Palynological studies from various basins suggest a warm humid/semi-humid subtropical climate during the middle and late Miocene, followed by gradual cooling during the early Pliocene (Xu et al., 2004; Kou et al., 2006; Xu et al., 2008; Xia et al., 2009; Jacques et al., 2011; Xing et al., 2012; Su et al., 2013). However, most of the research has focused on the late Miocene or late Pliocene and their age control was mainly based on stratigraphic correlation, so that precise chronological control is often lacking, which hinders our understanding of the climate evolution of the Yunnan region from the late Miocene through Pliocene.

The Zhaotong Basin is located in the southeastern margin of the Tibetan Plateau, and the climate of the region is controlled by the South Asian monsoon. Hence, the long, continuous sedimentary succession of the Zhaotong Basin potentially provides an excellent continental record to study the evolution history of the South Asian monsoon. Clay mineralogy is extensively used to reconstruct climate change, tectonic evolution, atmosphere-ocean circulation and other paleogeographic events (Chamley, 1989), and has been especially applied to the pre-Quaternary (Robert and Chamley, 1991; Ehrman, 1998; Winkler et al., 2002; Zhang and Guo, 2014; Zhang et al., 2015a, 2015b, 2016). Hence, we present the results of a study of changes in the clay mineral assemblages of a high-quality sedimentary sequence from the Zhaotong Basin. Our aims were to improve our understanding of the evolution of the South Asian monsoon from the late Miocene through Pliocene, and to determine the major driver.

2. Geological setting

The southeastern margin of the Tibetan Plateau is located between the eastern Himalayan syntaxis and Sichuan basin, spanning the latitudinal range from ~25° to ~33°N. It is characterized by rugged topography with a long-wavelength, and well-developed drainage and valleys which contrast with the steep southern, northern and eastern margins (Hoke et al., 2014). A portion of the plateau margin is of low relief, interpreted as a relict landscape, of at least early to middle Miocene age (Clark et al., 2005), which is incised by the modern Yangtze, Red and Lancang (Mekong) Rivers (Clark et al., 2004; Schoenbohm et al., 2006; Hoke et al., 2014). Along these major rivers, the mean elevation decreased gradually southeastwards from ~4–5 km to ~2–3 km, across a northeast-trending ~200–250-km-wide zone (Liu-Zeng et al., 2008). The southeastern margin of the Tibetan Plateau contains several lithospheric fragments, including the Indochina, Sibumasu, Songpan Graze and South China Blocks (Wang et al., 1998; Li et al., 2017).

The Zhaotong Basin is located in northeastern Yunnan Province, southwestern China, at the southeastern margin of the Tibetan Plateau, with an elevation of ~1900 to 2000 m (Fig. 1). The basin has an irregular, roughly oval shape, with a length of ~15 km from west to east, and covers an area of ~230 km^2 (Wang, 2010; Chang et al., 2015). It is one of the fault-related late Neogene basins in the Xianshuihe-Xiaojiang fault zone, one of the major fault zones fold belts of South China (Wang, 1998). Zhaotong Basin occupies the area from 26.8° to 28.5°N and from

102.8° to 105.3°E, from NE to SW, respectively. The basin is filled with late Miocene to Pliocene lacustrine or swampy deposits including clays, silts, peaty clays and lignite. The sedimentary sequence has a thickness of 200–300 m and is underlain by Emeishan basalts or Permian limestone (Wang et al., 2013). The cranium of a terminal Miocene hominoid (*L.* cf. *lufengensis*) was found in the locality of Shuitangba, an open-pit lignite mine located in the Zhaotong Basin (Ji et al., 2013).

2.1. Stratigraphy of borehole core ZK1

This study focuses on the record of borehole core (ZK1) (27°19′23.3″N, 103°44′17.6″E, with an elevation of ~1922 m), which was drilled within a thick part of the Zhaotong Basin, several hundred meters away from the Shuitangba hominoid-bearing site. The overall length of the core is 120 m, with the upper 111.6 m consisting of late Cenozoic sediments, and the base of Permian limestone (111.6–120 m) (Ji et al., 2013). A total of 780 samples at a ~2 cm spacing were obtained from the core.

The sedimentary sequence and field geological characteristics of the ZK1 borehole and be divided into eight stratigraphic units, which are described below.

Unit I (0–5.8 m) - Grayish-brown fine graval-containing sandy clay, gray silty clay, gray to dark gray slit, and gray to light gray graval. The gray silty clay contains massive brown-yellow limonite layers, which develop in aerobic conditions.

Unit II (5.8–22.4 m) - Dark green-gray clay with two interlayers containing freshwater bivalves. The fossil content is minor from 18.96–19.06 m, and the bivalves are < 1 cm in diameter. The interval from 19.5–19.7 m contains a large number of fossil bivalves, with dimensions of 3–5 cm.

Unit III (22.4–63.0 m) - Mainly green-gray silty clay with one interlayer of poor quality lignite (32.1–32.25 m), one clayey silt layer (32.5–32.6 m) and seven bivalve layers (24.0–24.5 m, 24.30–24.35 m, 25.50–25.55 m, 31.28–31.30 m, 31.95–32.05 m, 32.5–32.6 m, and 42.5–43.3 m).

Unit IV (63.0–64.7 m) - Dark brown peat with several interlayers of carbonaceous clay; occasional wood fragments and aquatic plants.

Unit V (64.7–72.1 m) - Dark brown carbonaceous clay with three interlayers of dark brown lignite. Correlation between other fossil and borehole sites was achieved using a distinctive lignite-peaty clay-lignite triplet; the hominoid fossils were found in the upper part of the peaty clay.

Unit VI (72.1–104.5 m) - Mainly dark gray lignite containing wood and aquatic plant remains.

Unit VII (104.5–111.6 m) - Mainly dark-gray to gray clay.

Unit VIII (111.6–120.0 m) - Bedrock of light gray Permain limestone.

2.2. Chronology

Detailed magnetostratigraphic and biostratigraphic studies of the ZK1 borehole, especially in the context of the hominoid-bearing strata, were reported by Ji et al. (2013). However, the new geomagnetic polarity timescale (GPTS) of ATNTS2012 (Hilgen et al., 2012) is used in this study (Fig. 2B, C), which is lightly different from the classic GPTS of CK95 (Cande and Kent, 1995) used in Ji et al. (2013). The minor differences between the two age models result from different age data of the two GPTS. Magnetostratigraphic results indicate ten normal magnetozones (N1–N6) and nine reverse magnetozones (R1–R5) in the ZK1 borehole, which can be correlated to the geomagnetic polarity timescale. We correct the R5 to C4r.1r-C4r.2r, which is more reasonable considering the pattern of sediment accumulation rates of the Zhaotong borehole sequence. Correlation of the recognized magnetozones to the geomagnetic polarity timescale (GPTS; Hilgen et al., 2012) aided by the biostratigraphic constraints, reveals that the Zhaotong Basin borehole sedimentary sequence spans the interval from late chron C2An.1n to the lower chron C4r.2r, which was confirmed by a detailed cyclostratigraphic study, constrained by the magnetostratigraphy. Correlation to the GPTS yielded 13 age control points (Table 1) and the sequence spans the interval from ~8.8 Ma to ~2.6 Ma. The age of other intervals within the section was estimated by extrapolating the sedimentation rate between age control points. In summary, both magnetostratigraphic and biostratigraphic data confirm that the studied sedimentary sequence is continuous and spans the interval from the late Miocene to the Pliocene.

2.3. Laboratory methods

2.3.1. Grain size analysis

All 780 samples were air-dried naturally in the laboratory. Samples were pretreated with 30% H_2O_2 and 10% HCl to remove organic matters and the carbonates, respectively. Deionized water was then added to reduce the acidity and the samples were left standing for 24 h; the supernatant was then removed and additional deionized water was added and the samples were left for standing for another 24 h. Subsequently, the supernatant was siphoned off using latex tubing and the samples were then dispersed for 10 min in an ultrasonic bath with 10 ml 10% $(NaPO_3)_6$ solution to aid dispersion. Grain-size distribution were measured using a Coulter LS 13 320 laser grain-size analyzer with a measurement range of 0.375–2000 μm in the Laboratory of Soil Geology and Environment, Institute of Geology and Geophysics, Chinese Academy of Sciences (IGGCAS). The < 2 μm fraction were taken to represent the proportion of clay.

2.3.2. Clay mineralogy analysis

For clay mineral analysis, 88 samples at a ~1.3 m spacing were selected. The samples were disaggregated in deionized water and treated with 20 ml of 10% H_2O_2 and then with 1 mol/L acetic acid to remove organic materials and carbonates, respectively. Then, the samples were washed with deionized water to remove excess ions and to aid deflocculation of the clays. The < 2 μm fraction was then separated according to the Stoke's Law; 1500 ml of solution from the top of the containers was removed and left to stand. The suspension containing the clay fraction was then split into three subsamples. One subsample was left untreated and the other two were saturated with $MgCl_2$ and KCl, respectively. Then clay minerals were then concentrated using centrifugation. The Mg-saturated subsample was then divided into three further subsamples, one was left untreated and glycerol (G) and liquid ethylene glycol (EG) added respectively to the two other subsamples. The resulting pastes were mounted on the calibrated recesses of glass slides to obtain oriented mounts. Five slides for each sample were prepared and were air-dried for X-ray diffraction (XRD) analysis. Then, K-saturated slides were heated at 120 °C, 300 °C and 550 °C for 2 h and analyzed at room temperature. The clay mineralogy was determined using a PANalytical diffractometer fitted with CuKα-radiation at 40 kV and 40 mA at the Laboratory of Soil Geology and Environment, IGGCAS.

Identification of clay minerals was based mainly on the position of the (001) series of basal reflections of a sample in seven states: air-dry (AD: original, Mg-saturated and K-saturated), saturated with glycerol (G) and ethylene glycol (EG), and heated at 120, 300 and 550 °C (Fig. 3), following the methods described by Zhang and Guo (2014). Smectite, illite and kaolinite were identified in the clay fractions of most samples. In addition, following Moore and Reynolds (1997), vermiculite was identified by its diffraction peaks at 14.2 Å (001), 7.1 Å (002), 4.7 Å (003), 3.5 Å (004); among these peaks, the 001 reflection peak is especially well-defined. Typically, samples are encountered that exhibit an intermediate peak between 14.5 and 17.7 Å with glycerol which collapses to 10 Å after K saturation in an air-dried state (Walker, 1958); in addition, the 14.2 Å vermiculite peak of Mg-, G- and EG- saturated samples remains constant. Moreover, these implied the 14.2 nm main peak in Fig. 3A–C may be vermiculite or 14 nm intergrade clays (e.g. hydroxyl-interlayered vermiculite (HIV)) (Chamley, 1989). As

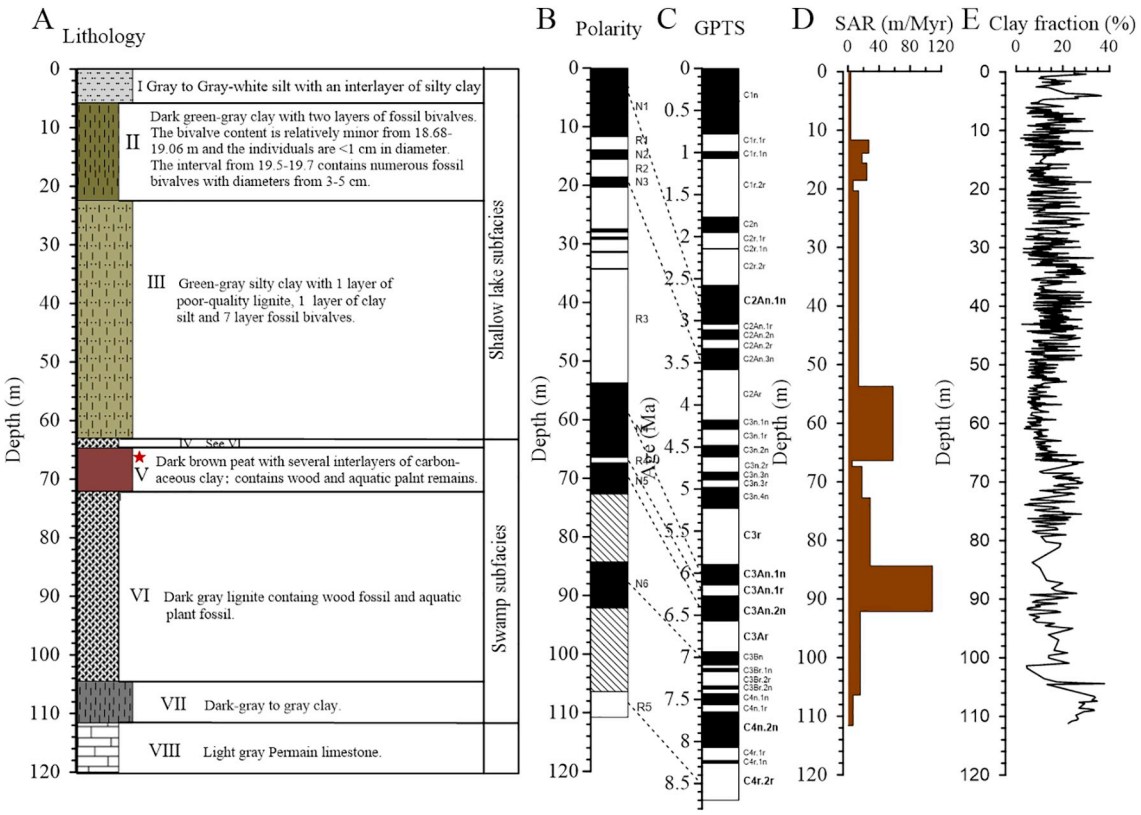

Fig. 2. A., Lithology, inferred depositional facies; B., magnetic polarity zonation (Ji et al., 2013) of the ZK1 borehole based on C the geomagnetic polarity timescale (ATNTS2012); (Hilgen et al., 2012) (the hatched areas indicate that less effective magnetic chronology data has been obtained); D., sediment accumulation rate; E., clay fraction content of samples from the ZK1 borehole.

Table 1
Magnetostratigraphic age control points for borehole ZK1, based on ATNTS2012 of Hilgen et al. (2012).

Datum	Depth (m)	Chron	Age (Ma)
1	11.66	C2An.1n	3.032
2	13.92	C2An.2n	3.116
3	15.58	C2An.2n	3.207
4	18.57	C2An.3n	3.330
5	20.31	C2An.3n	3.596
6	53.71	C3An.1n	6.033
7	66.41	C3An.1n	6.252
8	67.38	C3An.2n	6.436
9	72.7	C3An.2n	6.733
10	84.33	C3Bn	7.140
11	92.15	C3Bn	7.212
12	106.4	C4n	8.108
13	110.8	C4r	8.771

shown in Fig. 3A–C, the 14.2 nm main peak reduced but did not disappear on the K curve, and changed to a wide peak and, after 300 °C heating treatment, reduced to an asymmetric peak and moved to 10 nm position after 500 °C treatment, these phenomena suggested the presence of 1.4 nm intergrade clay (HIV) (Chamley, 1989).

For the coarse fraction, clay mineral abundance can be calculated by peak heights provided that the intensity of the diffraction pattern (generally expressed as peak area or peak height) of a mineral in a mixture is proportional to its concentrations (Zhang and Guo, 2014). The samples may contain a very small amount of hydroxy-interlayered vermiculite (HIV), which didn't show his diffraction peak in the EG-saturated samples, so there is no separation between the abundance of the HIV and vermiculite (Fig. 3A, C). Semi-quantitative estimates using peak area were obtained for the main clay mineral groups of vermiculite (including of HIV) (14.2 Å), smectite (17.0 Å), illite (10 Å) and kaolinite (7 Å) of glycolated curves using MacDiff software (Petschick, 2000). MacDiff offers conventional XRD profile-correlation processes (e.g. outliers, smoothing, divergence, alpha2-stripping) and the quantification of clay minerals is made using the integral of the diffraction peak area. The weighting factors introduced by Biscaye (1965) were used as follows: smectite: (HIV, vermiculite and kaolinite): mica group = 1:2:4 Biscaye (1965).

3. Results

3.1. Sedimentary facies

The lithology of the studied section is illustrated in Fig. 2. The section consists of eight lithological units, including two lignite layers (Section 2.1). Based on the detailed lithological information, observations of field geological characteristics and the clay fraction content, the sedimentary facies of Zhaotong Basin can be divided into two sections, which are described below.

The lower section (~111.6–63 m) consists of swamp sediments and includes four subfacies (Units VII–IV): Unit VII has a substantial clay content (mean of ~28.2%) and is a lacustrine facies; Unit VI consists mainly of dark gray lignite (mean clay fraction content of ~21.9%) and is a swamp subfacies; Unit V consists of dark brown carbonaceous clay (mean clay fraction of ~24.9%) and is a swamp subfacies; and Unit IV consists of dark brown peat (mean clay fraction content of ~8.55%) and is a swamp subfacies.

The upper section (0–63 m) consists mainly of lacustrine sediments. It comprises three subfacies (Units III–I). Unit III consists of green-gray silty clay with a mean clay fraction content of ~13% and is a shallow lake subfacies; Unit II consists of dark green-gray clay with a clay fraction content of ~20.2% and is a shallow lake subfacies; and Unit I, consisting of fine gravelly-sandy clay with a clay fraction content of

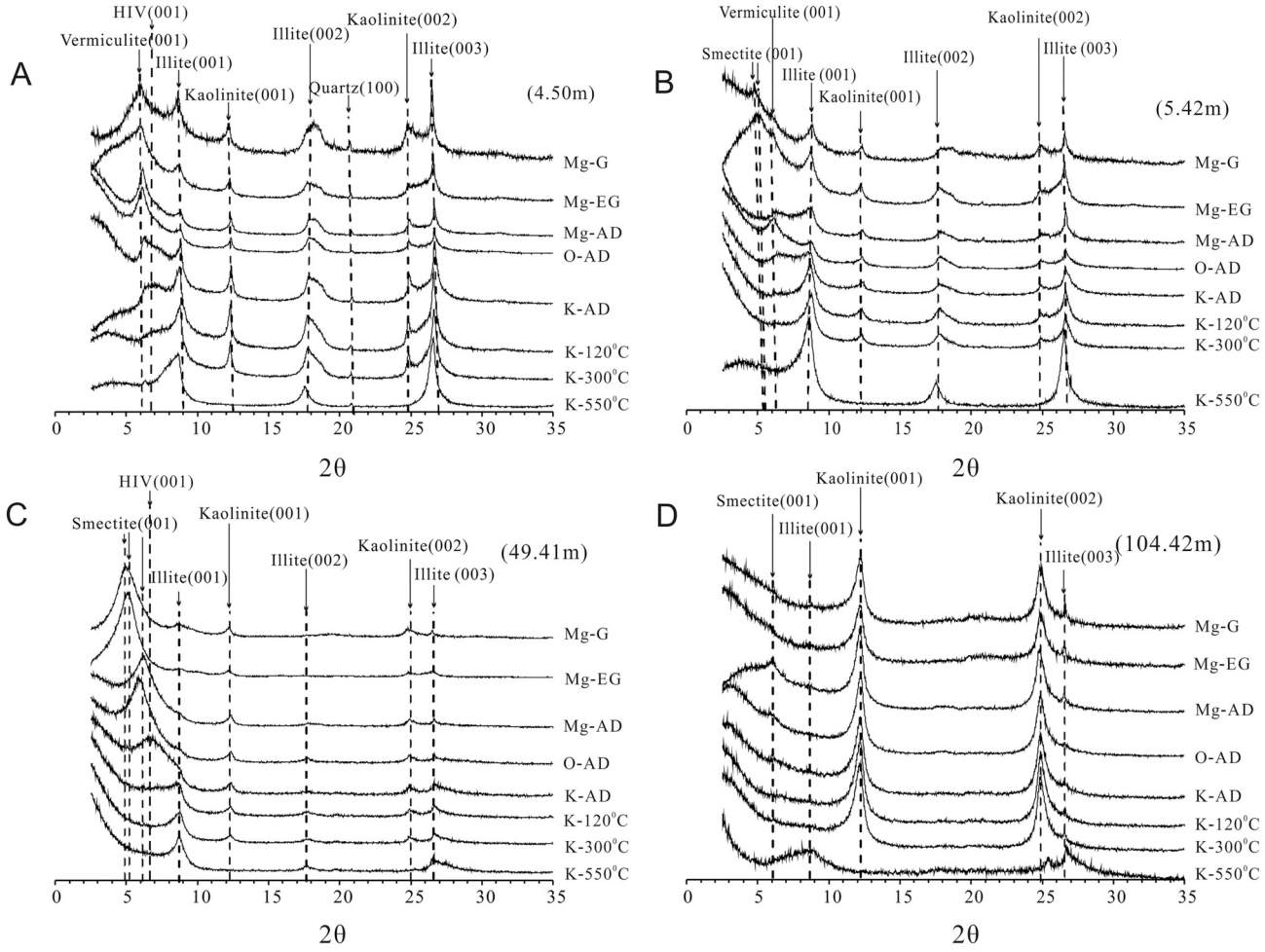

Fig. 3. X-ray diffractograms of typical samples from the ZK1 borehole. A., Clay-sized fractions with vermiculite, illite, kaolinite and HIV (hydroxyl-interlayered vermiculite); B., clay-sized fractions with vermiculite, illite, smectite, kaolinite; C., clay-sized fractions with illite, smectite, kaolinite and HIV; D., clay-sized fractions with illite, smectite, kaolinite.

~24.7%, and containing the massive limonite layers, is also a shallow lake subfacies.

The variations in the clay fraction content indicate that the hydrodynamic energy of the sedimentary environment gradually decreased, with little change in the amplitude of fluctuations, from the late Miocene to the Pliocene.

3.2. Clay mineralogy

Smectite, kaolinite, illite and vermiculite are the four dominant clay minerals in the sediments of borehole core ZK1 (Fig. 3). Smectite (0–91.7%) is the most abundant clay mineral with an average of ~62.9%; kaolinite (3.6–96.1%) is the next most abundant with an average of ~22.5%; and illite (0–49.9%) has a variable abundance with an average content of ~11.8%. From 0.24–5.24 m depth, the concentration of vermiculite (including of HIV) averages 42.1% and smectite is absent (Fig. 3A, B); from 5.02–107.20 m smectite, illite and kaolinite (Fig. 3C) are present but with variable concentrations; and from 107.2–111.2 m, kaolinite and smectite are present with a minor amount of illite.

Clay minerals concentrations are plotted versus depth in Fig. 4 and they vary with the sedimentary facies. Three main clay mineral assemblage zones are recognized within the entire borehole succession, with the boundaries equivalent to those of the sedimentary facies (Fig. 4). The characteristics of the zones are summarized in Table 2 and described below.

Zone I (111.6–63.0 m) is characterized by smectite (~43.60%), illite (~8.90%) and kaolinite (~41.92%). In addition, from bottom to top, the proportion of kaolinite decreases with the increased illite and smectite content. *Zone II (63.0–5.8 m)* is characterized by smectite (~78.5%), illite (~10.5%) and kaolinite (~11.0%), and the proportions are roughly constant with depth. *Zone III (5.8–0 m)* is characterized by smectite (~4.7%), illite (~38.2%), kaolinite (~14.9%) and vermiculite (including of HIV) (~42.1%).

4. Discussion

4.1. Formation of clay minerals and their climatic significance

Kaolinite, smectite, illite, vermiculite and trace HIV are present within the sediments of the Zhaotong Basin. In the Zhaotong Basin, the clay mineral assemblages of Zones I and II are the same (kaolinite, smectite and illite) but there are differences in the proportions of the clay minerals. In contrast, the clay mineral assemblages of Zone III comprise vermiculite (including of HIV), illite with trace kaolinite and smectite(Fig. 4). Both tectonic uplift and climate activities may influence the assemblages and contents of the clay mineral.

Permian limestone, Emeishan basalt and Triassic sandstone are the principal basement rocks of the Zhaotong Basin (Fig. 1B). The topography of the Zhaotong Basin is higher in the west than the east, and the outcrops in the west highlands are the main provenances of sediments in the Zhaotong Basin. As shown in Fig. 1B, the outcrops to the west of

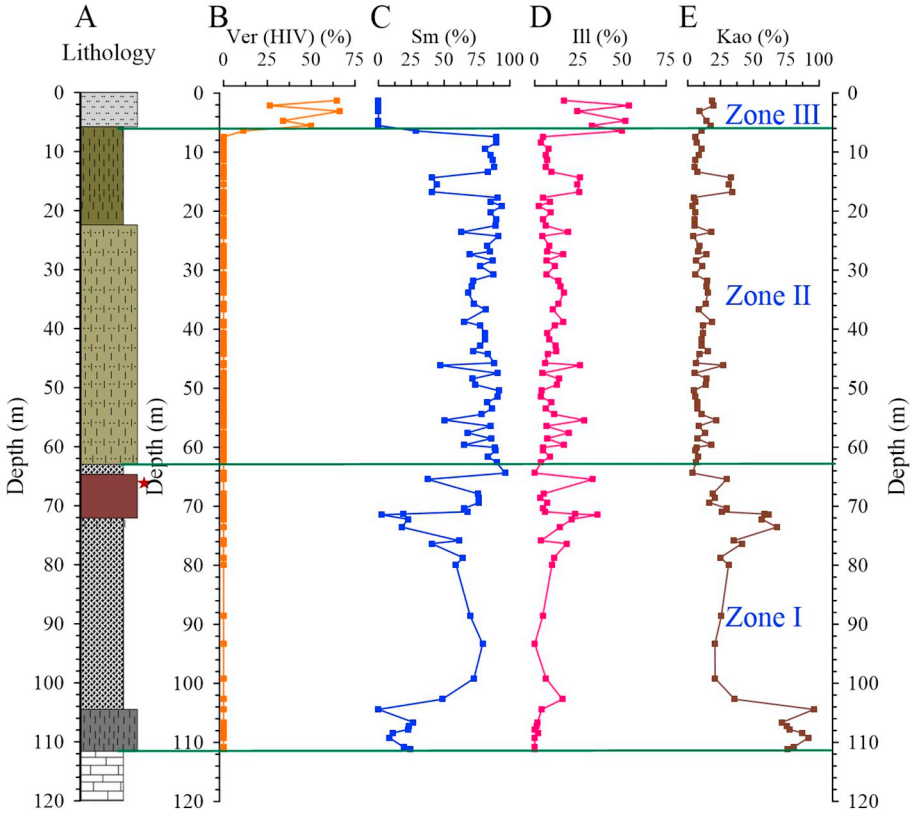

Fig. 4. Lithology and clay mineral composition of the samples from the ZK1 borehole in the Zhaotong Basin. The red star indicates the location of the cranium of the hominoid (*Lufengpithecus* cf. *lufengensis*). (For interpretation of the references to color in this figure legend, the reader is referred to the web version of this article.)

Table 2
Summary of the distributions of clay minerals within the ZK1 borehole.

Clay mineral (%)		All Samples	Zone I	Zone II	Zone III
Ver (HIV)	Range	0–64.7	0.0	0.0	11.3–64.7
	Median	2.9	0.0	0.0	42.1
Sm	Range	0–96.4	2.3–79.3	40.5–91.7	0–28.4
	Median	62.9	43.6	78.5	4.7
I	Range	0–53.8	0–35.8	3.4–26	16.8–53.8
	Median	11.8	8.9	10.5	38.2
Kao	Range	3.6–96.1	0–76.3	4.4–33.9	9.2–19.7
	Median	22.5	41.9	11.0	14.9

ZK1 are mainly the Emeishan basalt and Triassic sandstone. Moreover, the clay mineral assemblages of low elevations (1300–1900 m) Emeishan basalt-derived topsoil, and of late Miocene sediments at the Shuitangba site, are smectite, kaolinite and illite (Zhang et al., 2015a, 2015b, 2016), and the clay mineral of sandstone is mainly illite, similar to the clay mineral composition of the major part of borehole ZK1 (Zones I and Zone II) (Fig. 4). So we speculate that the clay mineral assemblages of the sediments of the Zhaotong Basin are relatively homogenous, mainly derived from the weathering of lower elevation Emeishan basalts and Triassic sandstone.

But in the Zone III there was a total disappearance of smectite with appearance of vermiculite(HIV), which we conjecture may be related to tectonic activities, diagenitic effects or climate change. Most of the active faults on the southeastern margin are strike slip faults, with minor transpression and transtension on the fault stepover, but there is no significant thickening (Leloup et al., 1993; Wang et al., 1998; Schoenbohm et al., 2006). The Zhaotong Basin is one of the fault-related basins in the Xianshuihe-Xiaojiang fault zone. The Xiaojiang faults, which are the nearest to the Zhaotong Basin, initiated at ~5 Ma (Wang et al., 2009), but there was no significant change of the clay mineral assemblages of ZK1 in the Zhaotong Basin during this period. Moreover, the strike slip faults in the southeastern margin of Tibetan Plateau may have influenced the initiation of the basin or change the direction of the water supply, but the lithology of the silty clay/clay silt and the continuous sedimentation (Fig.2) all suggest that the tectonic activities did not affect the development of ZK1 in the Zhaotong Basin. As well, the lithology of silts in Zone III, which is not significantly different with the underlying lithology; and the vermiculite (HIV) only occurs in Zone III, rather than in Zone II and I, which indicate that diagenetic effects did not result in the presence of vermiculite (HIV). A previous study showed that the clay minerals assemblage of high elevations (> 2200 m) Emeishan basalt-derived topsoil under cool and wet conditions is dominated by vermiculite (Zhang et al., 2015b). Therefore, the presence of vermiculate in Zone III may have resulted from the climate changes.

Nevertheless, the clay mineral assemblages of borehole ZK1 vary with the sedimentary facies (Figs. 4 and 5). The sedimentary characteristics (Fig. 2) indicate that the swamp facies have a high content of kaolinite and a low content illite, while the lacustrine facies have a high smectite content and a low kaolinite content (Fig. 4). The significantly correlations between the sedimentary facies and the proportions of clay minerals indicates that there were no significant changes in provenance area during the late Miocene through Pliocene. For the lacustrine-swamp environments, the temperature conditions were relatively stable, but there were substantial fluctuations in local humidity, suggesting that regional climatic conditions had a substantial effect on the sedimentary facies evolution (Zheng et al., 2008). The occurrence of shallow water/swamp sediments, the silty clay and clayey silt lithology, and continuity of sediment accumulation, all indicate that the sedimentary environment of the Zhaotong Basin was relatively constant from the late Miocene to the Pliocene. They also demonstrated that regional faulting did not affect the evolution of the sedimentary environment. Because the particle size of clay minerals is smaller

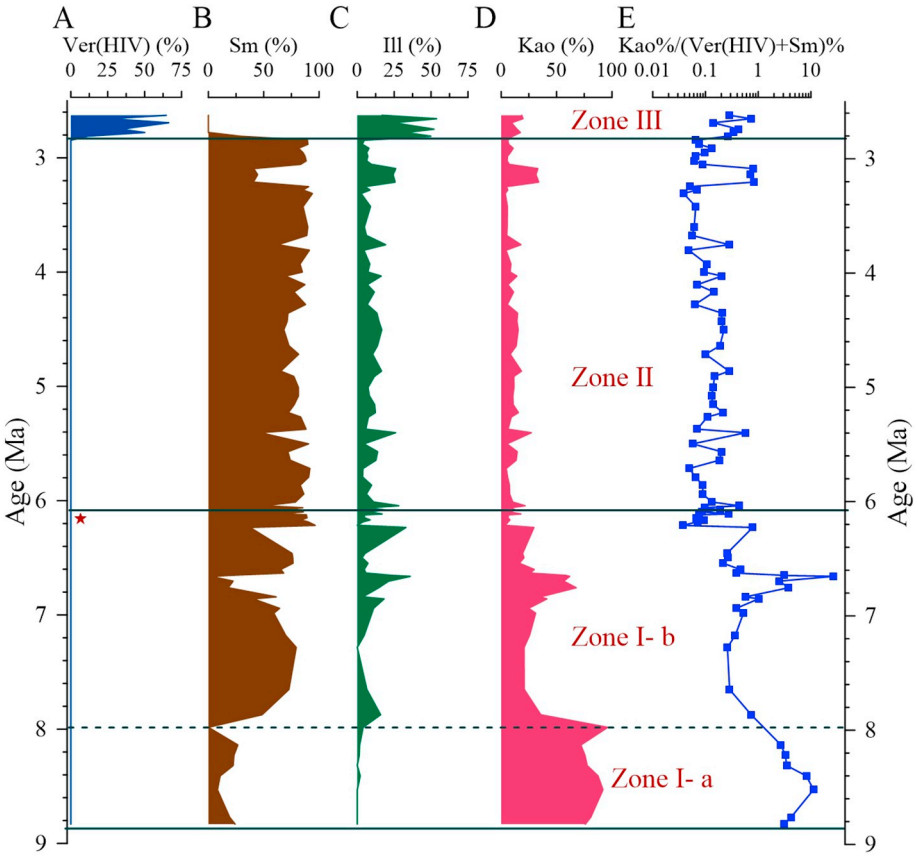

Fig. 5. Clay mineral composition of borehole ZK1 plotted versus age. (A–D), percentages of vermiculite (Ver(HIV)), smectite (Sm), illite (Ill) and kaolinite (Kao,) and (E) the ratio of kaolinite to smectite + Vermiculite(HIV). The star indicates the location of the cranium of the hominoid *Lufengpithecus* cf. *lufengensis*.

(< 2 μm) than other common sedimentary rock minerals (quartz, feldspar, amphiboles, biotite, muscovite, etc.), most clay minerals are transporting in water by suspension indicating that the grain size sorting has had little influence in the clay mineral deposits. Therefore, we assume that sedimentary environment and the clay mineral assemblages were predominately controlled by climate.

Individual clay minerals produce are formed by weathering under the specific conditions. In general, kaolinite is formed under a the humid climate with an acidic weathering environment with strongly leaching (Chamley, 1989; Tang et al., 2002). Kaolonite generally develops in highly hydrolytic weathering reactions and forms in warm humid climates. Smectite develops abundantly in areas of low reliefs where poor drainage prevents the removal of silica and alkaline and alkaline-earth ions and is generally linked to a warm climate with alternating humid and dry seasons. A cool and humid climate promotes development of podzols, which are characterized by free silica and highly degraded rock-derived clays, such as strongly altered illite, poorly defined vermiculite and mixed-layers vermiculite or smectite. Cool and humid conditions are responsible for the development of poorly-defined vermiculite and vermiculite (Chamley, 1989). Illite is formed at a relatively lower temperature and in weakly alkaline conditions, which promote the weathering of feldspar, mica and other aluminosilicate minerals and the loss of potassium. A very cold or hot, dry climate produces rock-derived minerals, with abundant illite (Chamley, 1989). Therefore, the relative proportions of vermiculite (HIV), smectite and kaolinite can be used as a proxy for climate proxy, with a high to low kaolinite / (vermiculite (HIV) + smectite) ratio (or Kao / (Ver(HIV) + Sm) ratio) is indicative of a gradient from warm and humid to cold and dry climates.

4.2. Climate changes in the Zhaotong Basin during the late Miocene through Pliocene inferred from clay mineral assemblages

Time series of clay mineral proportions and of the ratio of kaolinite to smectite + illite are illustrated in Fig. 5. The inferred climatic significance of the three clay mineral assemblages as described as follows:

Zone I (111.6–63 m, 8.8–6.2 Ma). The site was occupied by a swamp environment. The zone can be divided into two subzones (Figs. 4, 5): *Subzone I-a (111.6–104.5 m, 8.8–8.0 Ma)* has a relatively high kaolinite content and the lowest illite content (Fig. 5D, E) and high values of the Kao / (Ver(HIV) + Sm) ratio, indicating a very warm and humid environment. Compared to the preceding subzone, *subzone I-b (104.5–63 m, 8.0–6.2 Ma)* has a lower kaolinite proportion and Kao / (Ver(HIV) + Sm) and an increased content of illite and smectite, indicating a decrease in regional temperature and humidity.

Zone II (63.0–5.8 m, 6.2–2.8 Ma). The site was occupied by a shallow lake environment. The clay mineral assemblages are dominated by smectite and have a low kaolinite content and a low Kao / (Ver (HIV) + Sm) ratio, indicating that the climate became cooler and less humid compared to Zone I.

Zone III (5.8–0 m, 2.8–2.6 Ma). The site was occupied by a shallow lake environment. Vermiculite (HIV) is present, smectite disappears, and the kaolinite content is roughly constant. The replacement of smectite by vermiculite may come from the erosions of the high-elevation Emeishan basalt-derived topsoil with high vermiculite (HIV) content and the less weathered materials with high illite content, which may relate to the increased erosion rates at 2–4 Ma ago caused by the abrupt global cooling (Zhang et al., 2001). These characteristics indicate a much colder and humid climate than during the preceding zone. The lower section (111.6–63 m) of the sediments from Zhaotong Basin consists of dark gray lignite or peaty clay, interpreted as swamp

facies, indicating that the climate was warm and humid which produced a substantial amount of organic matter. Because of the high water table, the organic matter has well preserved, resulting in the formation of peat and lignite. In addition, a recent clay mineralogical analysis of the same horizon demonstrated the occurrence of a mild, warm and humid climate in the Zhaotong Basin during the late Neogene (Zhang et al., 2016). This conclusion is also supported by pollen evidence from the same site: the pollen assemblages during this interval indicate the presence of typical evergreen broadleaved forest with grasses in open spaces of the understory or at the woodland edge (Chang et al., 2015).

The upper section (0–63 m) of borehole core ZK1 is mainly a shallow lake subfacies. Huang et al. (2015) described a new species of aquatic plant, *Euryale yunnanensis*, dated to the late Miocene, from seed remains in the Zhaotong Basin. The modern equivalent lives in shallow lakes and swamps with stable hydrological conditions. Thus, the authors hypothesize that a shallow lake and/or swarmp environment was present close to Shuitangba in the Zhaotong Basin.

Fossils remains of the hominoid *Lufengpithecus* cf. *lufengensis*, with a late Miocene age of ~6.2 Ma, was found in the Shuitangba (STB) section (Fig. 4) in the Zhaotong Basin (Ji et al., 2013; Chang et al., 2015; Zhang et al., 2016), only ~580 m from the site of borehole ZK1. Zhang et al. (2016) suggested that *Lufengpithecus* cf. *lufengensis* lived in a mild, warm and humid lacustrine or swamp environment. The fossil was discovered at the boundary between Zones I and II, the long sequence of climate recorded shows that the terminal Miocene hominoid (*Lufengpithecus* cf. *lufengensis*) was present at the climate turning point from relatively warm and humid to relatively cool and humid in the Zhaotong Basin.

In summary, the variations of the clay mineral assemblages in borehole core ZK1 indicate that the climate of the Zhaotong Basin changed from warm and humid in the late Miocene to cool and humid in the very late Miocene through Pliocene, and then to cold and humid in the very late Pliocene.

4.3. Comparison with records from elsewhere and possible driving mechanisms of the South Asian monsoon

To better understand the evolution of the South Asian monsoon during the late Miocene through Pliocene, we compared our record of the kaolinite/(smectite + vermiculite(HIV)) ratio from the Zhaotong Basin with selected paleoclimatic records from the south Asian monsoon region and elsewhere (Fig. 6). The changes in clay mineral assemblages in the Zhaotong Basin from the late Miocene through Pliocene reveal a pattern of climatic evolution from warm and humid to cold and humid, which suggests a gradual decrease in the intensity of the South Asian monsoon in the Zhaotong Basin during this interval. This conclusion is supported by other climatic records from the South Asian monsoon region. The $\delta^{18}O$ record from the Siwalik Group in northern Pakistan shows a shift in the latest Miocene, probably corresponding to a major change in the source of water vapor (Fig. 6B) (Quade et al., 1989). Furthermore, changes in the percentages of grassland tropical forest taxa of a sequence of fluvial sediments of the Siwalik Group in the southern part of Himalaya a change from a wet monsoonal forest before 8.5 Ma to dry forest at 7 Ma, and then to savannah at 6 Ma (Hoorn et al., 2000). A $\delta^{18}O$ record from the Himalayan Foreland Basin in Northern India, spanning the interval from ~12–2 Ma, indicates a trend of decreasing precipitation (Sanyal et al., 2005). All these records suggest that the South Asian monsoon weakened progressively from the late Miocene to the Pliocene.

However, the abundance of the planktonic foraminifer *Globigerina bulloides* at ODP Site 722 in the Arabian Sea increased sharply at ~8.5 Ma, indicating the significant intensification of the South Asian monsoon system at ~8.5 Ma, which is consistent with a record of *Actinomma* spp. (Kroon et al., 1991; Prell and Kutzbach, 1992; An et al., 2001). Recent studies have testified that at ~8.5 Ma the seafloor of the Owen Ridge was significantly uplifted above the lysocline, inducing the dominance of *G. bulloides* at about 8.5 Ma, which was unrelated to Asian monsoon intensification (Huang et al., 2007; Rodriguez et al., 2014). These changes in foraminiferal abundances during the late Miocene suggest a change in preservation conditions rather than climatic change (Rodriguez et al., 2014).

Based on sedimentary records from the Arabian Sea (Kroon et al., 1991), the evolution of the South Asian monsoon has long been related to the uplift of the Himalayan–Tibetan Plateau (Molnar et al., 1993; An et al., 2001; Liu and Yin, 2002; Abe et al., 2003; Zheng et al., 2004; Fang et al., 2007). Previous studies have concluded that the South Asian monsoon commenced or was intensified substantially at ~8 Ma, in response to Himalayan-Tibetan uplift to an elevation at least one-half of its modern elevation (Prell and Kutzbach, 1992; Rea et al., 1998). However the factors controlling the abundance of *G. bulloides* since 8.5 Ma are still debated, and it is difficult to conclude from this line of evidence alone that the South Asian monsoon was strongly intensified since the late Miocene. Moreover, recent research on IODP Site U1456 in the Arabian Sea suggests that the South Asian monsoon was persistently weaker from ~10.2–3.1 Ma, and thus did not intensify at ~8 Ma, in contradiction with several previous studies (Tripathi et al., 2017). As well, Hoke et al. (2014) examined the topographic evolution of the southeastern margin of the Tibetan Plateau during the Cenozoic, and concluded that the southeastern margin of the Tibetan plateau was at its modern altitude as early as the late Eocene, with an elevation of 3.3 km as far south as the northern third of China's Yunnan Province (Hoke et al., 2014). In fact, there is a growing consensus that much of the central and southern Tibetan Plateau was uplifted close to its modern altitude before the Middle Miocene (Decelles et al., 2007; Liu et al., 2015; Xu et al., 2017).

The recent reconstructions of sea-surface temperature (SST) for the western Arabian Sea since the middle Miocene indicate a long-term ocean cooling since 14.8 Ma and a major drop in SST in the period of 11–10 Ma, but a quite flat trend between 8 and 6 Ma (Zhuang et al., 2017) (Fig. 6C). Also, some opinions suggest that an orographic high such as the Himalaya may be more important than the elevation and/or extent of the entire plateau in shaping modern South Asian monsoon circulation (Boos and Kuang, 2010; Ding et al., 2017). The uplift of the Himalaya-Tibetan Plateau may have intensified the South Asian monsoon, but it cannot explain its apparent weakening or the flat trend of SST during the late Miocene through Pliocene, as evidenced by the clay mineral assemblages from the Zhaotong Basin, fluvial sediments of the Siwalik Group, and various marine records.

A pronounced climatic trend is evidenced by the clay mineral assemblages of the Zhaotong Basin: from warm and humid conditions in the late Miocene (~8.9–6.2 Ma), to cool and humid conditions in the very late Miocene through Pliocene (~6.2–2.8 Ma), and then to cold and humid conditions in the very late Pliocene (~2.8 Ma). This trend indicates that the South Asian monsoon decreased in intensity during this interval. The late Miocene vegetation transition represents a climate change from wet monsoonal forest before 8.5 Ma, to dry monsoonal forest at 7 Ma, and then to savannah at 6 Ma (Hoorn et al., 2000; Badgley et al., 2008). Herbert et al. (2016) inferred a sustained and synchronous late Miocene cooling of both hemispheres which culminated with ocean temperatures decreasing to near-modern values from ~7 to ~5.4 Ma, based on a set of globally distributed sea surface temperature records. They concluded that a global forcing mechanism was needed to explain the observed late Miocene changes in climates and environments. Compared with the tropical Sea Surface Temperature record (Fig. 6D) (Herbert et al., 2016), we deduce that the climate change at the Zhaotong Basin was controlled by global cooling from the late Miocene. The global trend of a cooler late Cenozoic climate (Lariviere et al., 2012), which may have reduced the amount of water vapor in the atmosphere, would have weakened precession-related moisture cycles. Hence, global cooling (Zachos et al., 2001; Herbert et al., 2016) may have played a critical role in the evolution of the

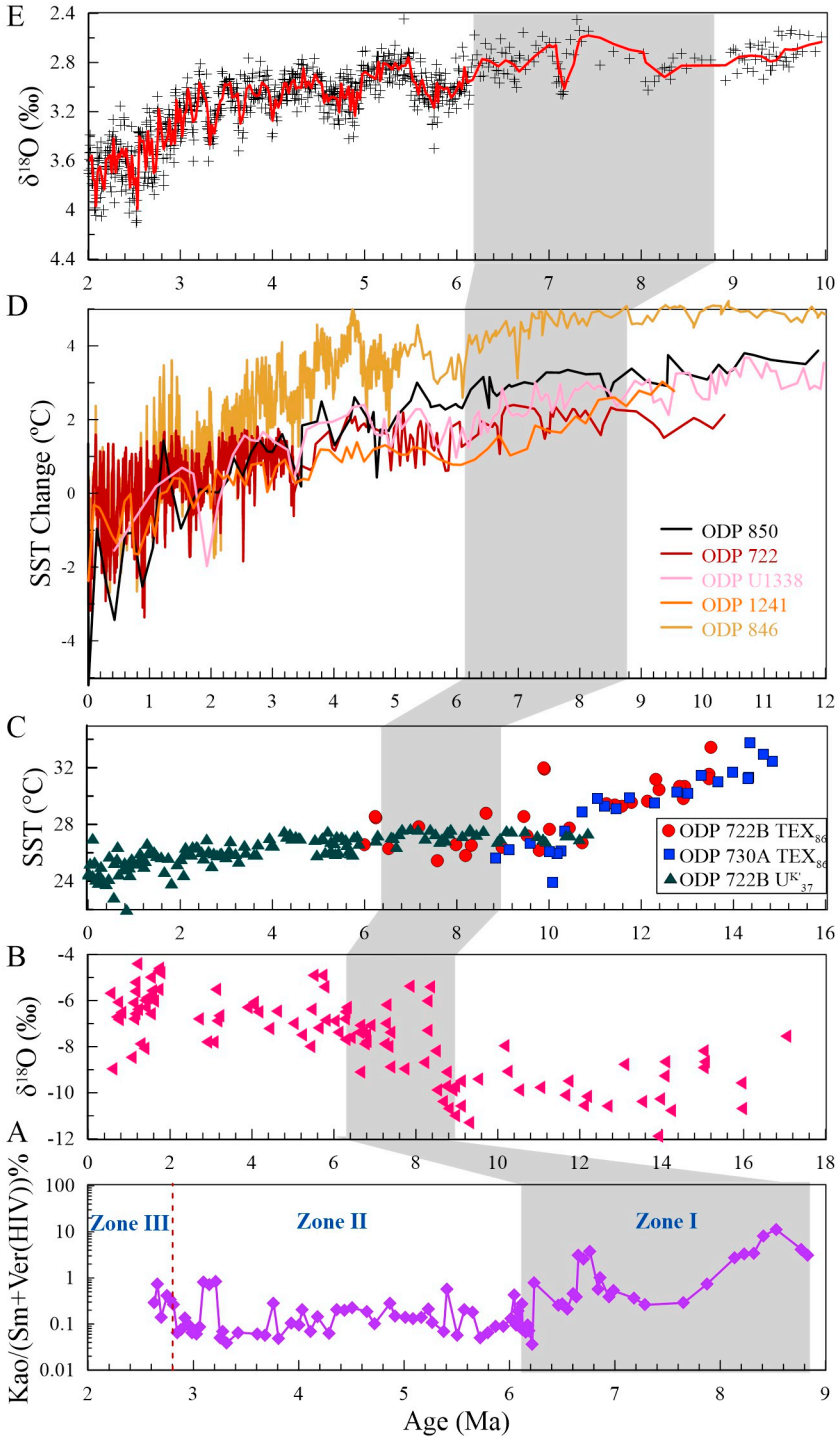

Fig. 6. A., Variation of Kao / (Sm + Ver(HIV))% ratio from the Zhaotong Basin; B., $\delta^{18}O$ record (PDB) of palaeosol carbonate nodules from the Siwalik Group in northern Pakistan (Quade et al., 1989); C., TEX_{86} sea-surface temperature (SSTs) at Ocean Drilling Program (ODP) Sites 722B and 730A (Zhuang et al., 2017) and $U^{K'}_{37}$ SSTs at Site 722B (Huang et al., 2007); D., tropical sea surface temperature record based on the alkenone unsaturation methods (Muller et al., 1998; Herbert et al., 2016); E., marine oxygen isotope record (Zachos et al., 2001).

South Asian monsoon evolution from the late Miocene through Pliocene.

In summary, the clay mineral assemblages of the Zhaotong Basin demonstrate that the intensity of the South Asian monsoon decreased from the late Miocene through the Pliocene. Although the possible role of Tibetan Plateau uplift in influencing this trend cannot be excluded, we conclude that ongoing global cooling and the expansion of the Northern Hemisphere ice sheets likely played the more important role in the evolution of the South Asian monsoon during this interval.

5. Conclusions

We have measured the variation of clay mineral assemblages from the late Miocene through the Pliocene in a high-quality sedimentary sequence accumulated in the Zhaotong Basin on the southeastern margin, of the Tibetan Plateau. The region is substantially affected by the modern South Asian monsoon. Smectite, kaolinite, illite and vermiculite (HIV) are the four main clay minerals identified. The variations in clay mineral assemblages and in clay-fraction content indicate that

the following stages in the climatic evolution of the Zhaotong Basin from the late Miocene through the Pliocene: a warm and humid climate from 8.8–6.2 Ma; a cool and humid climate from 6.2–2.8 Ma; and a relatively cold and humid climate from 2.8–2.62 Ma. These changes suggest the gradual weakening of the South Asian monsoon during this interval. Comparison of our results with paleoclimatic records from elsewhere in the South Asian monsoon region leads us to conclude that global cooling was likely the major driver of the evolution of the South Asian monsoon evolution during the late Miocene through Pliocene.

Acknowledgments

We thank Drs. Qinzhen Hao, Xinbo Gao, Zhilin He and Bin Hu from the Institute of Geology and Geophysics, Chinese Academy of Sciences for their constructive comments and helpful discussion. We are also grateful to the editor Paul Hesse, Thomas Algeo, and two anonymous reviewers for their constructive reviews and meaningful comments. This study was financially supported by the "Strategic Priority Research Program" of the Chinese Academy of Sciences (Grant No. XDB26000000), the National Natural Science Foundation of China (Grant Nos. 41722206, 41430531 and 41374072), and the Zhaotong Government.

Appendix A. Supplementary data

Supplementary data to this article can be found online at https://doi.org/10.1016/j.palaeo.2018.11.039.

References

Abe, M., Kitoh, A., Yasunari, T., 2003. An evolution of the Asian Summer Monsoon associated with mountain uplift-simulation with the MRI atmosphere-ocean coupled GCM. Numen 81 (5), 909–933. https://doi.org/10.2151/jmsj.81.909.

An, Z.S., Kutzbach, J.E., Prell, W.L., Porter, S.C., 2001. Evolution of Asian monsoons and phased uplift of the Himalaya-Tibetan plateau since Late Miocene times. Nature 411 (6833), 62. https://doi.org/10.1038/35075035.

Badgley, C., Barry, J.C., Morgan, M.E., Nelson, S.V., Behrensmeyer, A.K., Cerling, T.E., Pilbeam, D., 2008. Ecological changes in Miocene mammalian record show impact of prolonged climatic forcing. Proc. Natl. Acad. Sci. U. S. A. 105 (34), 12145–12149. https://doi.org/10.1073/pnas.0805592105.

Biasatti, D., Wang, Y., Gao, F., Xu, Y., Flynn, L., 2012. Paleoecologies and paleoclimates of late cenozoic mammals from Southwest China: evidence from stable carbon and oxygen isotopes. J. Asian Earth Sci. 44, 48–61. https://doi.org/10.1016/j.jseaes.2011.04.013.

Biscaye, P.E., 1965. Mineralogy and sedimentation of recent depth-sea clay in the Atlantic Ocean and adjacent seas and oceans. Geol. Soc. Am. Bull. 76, 803–832.

Boos, W.R., Kuang, Z., 2010. Dominant control of the South Asian monsoon by orographic insulation versus plateau heating. Nature 463, 218–222. https://doi.org/10.1038/nature08707.

Brunet, M., 2010. Two new Mio-Pliocene Chadian hominids enlighten Charles Darwin's 1871 prediction. Philos. Trans. R. Soc. Lond. 365 (1556), 3315–3321. https://doi.org/10.1098/rstb.2010.0069.

Cande, S.C., Kent, D.V., 1995. Revised calibration of the geomagnetic polarity timescale for the Late Cretaceous and Cenozoic. J. Geophys. Res. Solid Earth 100, 6093–6095.

Cerling, T.E., Wang, Y., Quade, J., 1993. Expansion of C4 ecosystems as an indicator of global ecological change in the late Miocene. Nature 361 (6410), 344–345. https://doi.org/10.1038/361344a0.

Cerling, T.E., Harris, J.M., MacFadden, B.J., Leakey, M.G., Quade, J., Eisenmann, V., Ehleringer, J.R., 1997. Global vegetation change through the Miocene/Pliocene boundary. Nature 389 (6647), 153. https://doi.org/10.1038/38229.

Chamley, H., 1989. In: Chamley, H. (Ed.), Clay Sedimentology, pp. 21–51 (Ch.2).

Chang, L., Guo, Z.T., Deng, C.L., Wu, H.B., Ji, X.P., Zhao, Y., et al., 2015. Pollen evidence of the palaeoenvironments of *Lufengpithecus lufengensis* in the Zhaotong Basin, southeastern margin of the Tibetan Plateau. Palaeogeogr. Palaeoclimatol. Palaeoecol. 435, 95–104. https://doi.org/10.1016/j.palaeo.2015.06.007.

Clark, M.K., Schoenbohm, L.M., Royden, L.H., Whipple, K.X., Burchfiel, B.C., Zhang, X., et al., 2004. Surface uplift, tectonics, and erosion of eastern tibet from large-scale drainage patterns. Tectonics 23 (1). https://doi.org/10.1029/2002TC001402.

Clark, M.K., House, M.A., Royden, L.H., Whipple, K.X., Burchfiel, B.C., Zhang, X., et al., 2005. Late cenozoic uplift of southeastern Tibet. Geology 33 (6), 525. https://doi.org/10.1130/G21265.1.

Clift, P.D., Hodges, K.V., Heslop, D., Hannigan, R., Long, H.V., Calves, G., 2008. Correlation of Himalayan exhumation rates and Asian monsoon intensity. Nat. Geosci. 1 (12). https://doi.org/10.1038/ngeo1351.

Decelles, P.G., Quade, J., Kapp, P., Fan, M., Dettman, D.L., Ding, L., 2007. High and dry in central Tibet during the Late Oligocene. Earth Planet. Sci. Lett. 253 (3), 389–401. https://doi.org/10.1016/j.epsl.2006.11.001.

Ding, L., Spicer, R.A., Yang, J., Xu, Q., Cai, F., Li, S., et al., 2017. Quantifying the rise of the himalaya orogen and implications for the South Asian monsoon. Geology 45 (G38583.1), G38583.1. https://doi.org/10.1130/G38583.1.

Ehrman, W., 1998. Implications of late Eocene to early Miocene clay mineral assemblages in McMurdo Sound (Ross Sea, Antarctica) on paleoclimate and ice dynamics. Palaeogeogr. Palaeoclimatol. Palaeoecol. 139 (3–4), 213–231. https://doi.org/10.1016/S0031-0182(97)00138-7.

Fang, X.M., Xu, X.H., Song, C.H., Han, W.X., Meng, Q.Q., Torii, M., 2007. High resolution rock magnetic records of Cenozoic sediments in the Linxia Basin and their implications on drying of Asian inland. J. Quat. Sci. 27 (6), 989–1000 (In Chinese with English abstract).

Flower, B., Kennett, J., 1993. Middle Miocene ocean-climate transition: High-resolution oxygen and carbon isotopic records from Deep Sea Drilling Project Site 588A, southwest Pacific. Paleoceanography 8 (6), 811–843. https://doi.org/10.1029/93PA02196.

Guo, Z., Peng, S., Hao, Q., Biscaye, P.E., An, Z., Liu, T., 2004. Late Miocene-Pliocene development of Asian aridification as recorded in the Red-Earth Formation in northern China. Glob. Planet. Chang. 41 (3–4), 135–145. https://doi.org/10.1016/j.gloplacha.2004.01.002.

Gupta, A.K., Srinivasan, M.S., 1992. *Uvigerina proboscidea* abundances and paleoceanography of the northern Indian Ocean DSDP site 214 during the Late Neogene. Mar. Micropaleontol. 19 (4), 355–367. https://doi.org/10.1016/0377-8398(92)90038-L.

Gupta, A.K., Joseph, S., Thomas, E., 2001. Species diversity of Miocene deep-sea benthic foraminifera and watermass stratification in the northeastern Indian Ocean. Micropaleontology 47 (2), 111–124. https://doi.org/10.2307/1486055.

Herbert, T.D., Lawrence, K.T., Tzanova, A., Peterson, L.C., Caballerogill, R., Kelly, C.S., 2016. Late miocene global cooling and the rise of modern ecosystems. Nat. Geosci. 9 (11). https://doi.org/10.1038/NFEO2813.

Hilgen, F.J., Lourens, L.J., van Dam, J.A., 2012. The Neogene Period. In: Gradstein, F., Ogg, J.G., Schmitz, M.D., Ogg, G.M. (Eds.), The Geologic Time Scale 2012, pp. 923–978.

Hoke, G.D., Jing, L.Z., Hren, M.T., Wissink, G.K., Garzione, C.N., 2014. Stable isotopes reveal high southeast Tibetan Plateau margin since the Paleogene. Earth Planet. Sci. Lett. 394 (10), 270–278. https://doi.org/10.1016/j.epsl.2014.03.007.

Hoorn, C., Ohja, T., Quade, J., 2000. Palynological evidence for vegetation development and climatic change in the Sub-Himalayan Zone (Neogene, Central Nepal). Palaeogeogr. Palaeoclimatol. Palaeoecol. 163 (3), 133–161. https://doi.org/10.1016/S0031-0182(00)00149-8.

Huang, Y.S., Clemens, C., Liu, W., Wang, Y., Prell, W.L., 2007. Large-scale hydrological change drove the late Miocene C4 plant expansion in the Himalayan foreland and Arabian Peninsula. Geology 35 (6), 531. https://doi.org/10.1130/G23666A.1.

Huang, Y., Ji, X., Su, T., Wang, L., Deng, C., Li, W.H., et al., 2015. Fossil seeds of Euryale (Nymphaeaceae) indicate a lake or swamp environment in the late Miocene Zhaotong Basin of southwestern China. Sci. Bull. 60 (20), 1768–1777. https://doi.org/10.1007/s11434-015-0870-4.

Jacques, F.M.B., Guo, S.X., Su, T., Xing, Y.W., Huang, Y.J., Liu, Y.S., Ferguson, D.K., Zhou, Z.K., 2011. Quantitative reconstruction of the Late Miocene monsoon climates of southwest China: a case study of the Lincang flora from Yunnan Province. Palaeogeogr. Palaeoclimatol. Palaeoecol. 304, 318–327. https://doi.org/10.1016/j.palaeo.2010.04.014.

Ji, X., Jablonski, N.G., Su, D.F., Deng, C., Flynn, L.J., You, Y., Kelley, J., 2013. Juvenile hominoid cranium from the terminal Miocene of Yunnan, China. Chin. Sci. Bull. 58 (31), 3771–3779. https://doi.org/10.1007/s11434-013-6021-x.

Kou, X.Y., Ferguson, D.K., Xu, J.X., Wang, Y.F., Li, C.S., 2006. The reconstruction of paleovegetation and paleoclimate in the late Pliocene of west Yunnan, China. Clim. Chang. 77, 431–448. https://doi.org/10.1007/s10584-005-9039-5.

Kroon, D., Steens, T.N.F., Troelstra, S.R., 1991. Onset of Monsoonal Related Upwelling in the Western Arabian Sea as Revealed by Planktonic Foraminifers. Proceeding of the Ocean Drilling Program Scientific Results 117. pp. 257–263. https://doi.org/10.2973/odp.proc.sr.117.126.1991.

Lariviere, J.P., Ravelo, A.C., Crimmins, A., Dekens, P.S., Ford, H.L., Lyle, M., et al., 2012. Late Miocene decoupling of oceanic warmth and atmospheric carbon dioxide forcing. Nature 486 (7401), 97–100. https://doi.org/10.1038/nature11200.

Leloup, P.H., Harrison, T.M., Ryerson, F.J., Chen, W., Qi, L., Tapponnier, P., et al., 1993. Structural, petrological and thermal evolution of a tertiary ductile strike-slip shear zone, Diancang Shan, Yunnan. J. Geophys. Res. Solid Earth 98 (B4), 6715–6743. https://doi.org/10.1029/92JB02791.

Li, S.H., Advokaat, E.L., van Hinsbergen, D.J.J., Koymans, M., Deng, C.L., Zhu, R.X., 2017. Paleomagnetic constraints on the Mesozoic-Cenozoic paleolatitudinal and rotational history of Indochina and South China: review and updated kinematic reconstruction. Earth Sci. Rev. 171, 58–77. https://doi.org/10.1016/j.earscirev.2017.05.007.

Liu, X., Yin, Z.Y., 2002. Sensitivity of East Asian monsoon climate to the uplift of the Tibetan Plateau. Palaeogeogr. Palaeoclimatol. Palaeoecol. 183 (3), 223–245. https://doi.org/10.1016/S0031-0182(01)00488-6.

Liu, X., Hui, S., Miao, Y., Dong, B., Yin, Z.Y., 2015. Impacts of uplift of northern Tibetan Plateau and formation of Asian inland deserts on regional climate and environment. Quat. Sci. Rev. 116, 1–14. https://doi.org/10.1016/j.quascirev.2015.03.010.

Liu-Zeng, J., Tapponnier, P., Gaudemer, Y., Ding, L., 2008. Quantifying landscape differences across the Tibetan plateau: implications for topographic relief evolution. J. Geophys. Res. Earth Surf. 113 (F4). https://doi.org/10.1029/2007JF000897.

Molnar, P., England, P., Martiod, J., 1993. Mantle dynamics, uplift of the Tibetan Plateau and the Indian monsoon development. Rev. Geophys. 34, 357–396. https://doi.org/10.1029/93RG02030.

Moore, D.M., Reynolds Jr., R.L., 1997. X-ray Diffraction and the Identification and Analysis of Clay Minerals, Second edition. Oxford University Press, Oxford, New

York.
Muller, P.J., Krist, G., Ruhland, G., von Storch, I., Rosell-Mele, A., 1998. Calibration of the alkenone paleotemperature index $U^{K'}_{37}$ on core-tops from the eastern South Altantic and the global ocean (60° N-60° S). Geochim. Cosmochim. Acta 62, 1757–1772. https://doi.org/10.1016/S0016-7037(98)00097-0.
Patnaik, R., Gupta, A.K., Naidu, P.D., Yadav, R., Bhattacharyya, A., Kumar, M., 2012. Indian monsoon variability at different time scales: marine and terrestrial proxy records. Proc. Indian Natl. Sci. Acad. 78, 535–547.
Petschick, R., 2000. MacDiff 4.2.2 [Online]. http://servermac.geologie.un-frankfurt.de/Rainer.html.
Prell, W.L., Kutzbach, J.E., 1992. Sensitivity of the Indian monsoon to forcing parameters and implications for its evolution. Nature 360 (6405), 647–652. https://doi.org/10.1038/360647a0.
Prell, W.L., Murray, D.W., Clemens, S.C., Anderson, D.M., 1993. Evolution and Variability of the Indian Ocean Summer Monsoon: Evidence From the Western Arabian Sea Drilling Program. 70. pp. 447–469. https://doi.org/10.1029/GM070p0447.
Quade, J., Cerling, T.E., Bowman, J.R., 1989. Development of Asian monsoon revealed by marked ecological shift during the latest Miocene in northern Pakistan. Nature 342 (6246), 163–166. https://doi.org/10.1038/342163a0.
Quade, J., Cater, J.M.L., Ojha, T.P., Harrison, T.M., 1995. Late miocene environmental change in nepal and the northern indian subcontinent: stable isotopic evidence from paleosols. Geol. Soc. Am. Bull. 107 (12), 1381–1397. https://doi.org/10.1130/0016-7606(1995)107<1381:lmecin>2.3.co;2.
Ramstein, G., Fluteau, F., Besse, J., Joussaume, S., 1997. Effect of orogeny, plate motion and land–sea distribution on Eurasian climate change over the past 30 million years. Nature 386 (6627), 788–795. https://doi.org/10.1038/386788a0.
Rea, D.K., Snoeckx, H., Joseph, L.H., 1998. Late Cenozoic Eolian deposition in the North Pacific: Asian drying, Tibetan uplift, and cooling of the Northern Hemisphere. Paleoceanography 13 (3), 215–224. https://doi.org/10.1029/98PA00123.
Reuter, M., Kern, A.K., Harzhauser, M., Kroh, A., Piller, W.E., 2013. Global warming and South Indian monsoon rainfall-lessons from the Mid-Miocene. Gondwana Res. 23 (3), 1172–1177. https://doi.org/10.1016/j.gr.2012.07.015.
Robert, C., Chamley, H., 1991. Development of early Eocene warm climates, as inferred from clay mineral variations in oceanic sediments. Palaeogeogr. Palaeoclimatol. Palaeoecol. 89 (4), 315–331. https://doi.org/10.1016/0921-8181(91)90114-C.
Rodriguez, M., Chamot-Rooke, N., Huchon, P., Fournier, M., Delescluse, M., 2014. The Owen Ridge uplift in the Arabian Sea: Implications for the sedimentary record of Indian monsoon in Late Miocene. Earth Planet. Sci. Lett. 394, 1–12. https://doi.org/10.1016/j.epsl.2014.03.011.
Sanyal, P., Bhattacharya, S.K., Kumar, R., Ghosh, S.K., Sangode, S.J., 2004. Mio–Pliocene monsoonal record from himalayan foreland basin (Indian Siwalik) and its relation to vegetational change. Palaeogeogr. Palaeoclimatol. Palaeoecol. 205 (1), 23–41. https://doi.org/10.1016/j.palaeo.2003.11.013.
Sanyal, P., Bhattacharya, S.K., Prasad, M., 2005. Chemical diagenesis of Siwalik sandstone: isotopic and mineralogical proxies from Surai Khola section, Nepal. Sediment. Geol. 180 (1), 57–74. https://doi.org/10.1016/j.sedgeo.2005.06.005.
Schoenbohm, L.M., Burchfiel, B.C., Liangzhong, C., 2006. Propagation of surface uplift, lower crustal flow, and Cenozoic tectonics of the Southeast margin of the Tibetan plateau. Geology 34 (10), 813–816. https://doi.org/10.1130/G22679.1.
Shackleton, H.J., Hall, M., Pate, D., 1995. Pliocene stable isotope stratigraphy of Site 846. Proc. Ocean Drill. Program Sci. Results 138, 337–355. https://doi.org/10.2973/odp.proc.sr.138.117.1995.
Su, T., Jacques, F.M.B., Spicer, R.A., Liu, Y.S., Huang, Y.J., Xing, Y.W., Zhou, Z.K., 2013. Post-Pliocene establishment of the present monsoonal climate in SW China: evidence from the late Pliocene Longmen megaflora. Clim. Past 9, 1911–1920. https://doi.org/10.5194/cp-9-1911-2013.
Tang, Y.J., Jia, J.Y., Xie, X., 2002. Environment significance of clay minerals. Earth Sci. Front. 9 (2), 337–344 (In Chinese with English abstract).
Tripathi, S., Tiwari, M., Lee, J., Khim, B.K., 2017. First evidence of denitrification vis-à-vis monsoon in the Arabian Sea since Late Miocene. Sci. Rep. 7, 43056. https://doi.org/10.1038/srep43056.
Walker, G.F., 1958. Reactions of expanding lattice minerals with glycerol and ethylene glycol: Clay Miner. Bulletin 3, 302–313. https://doi.org/10.1180/claymin.1958.003.20.05.
Wang, J.Z., 2010. Preliminary evaluation on exploration prospect of CBM resources of the Neogene lignite in Shaotong Basin. Coalbed Methane Sci. Environ. Econ. Eval. 7 (2), 3–6 (In Chinese with English abstract).
Wang, E., Burchfiel, B.C., Royden, L.H., Chen, L., Chen, J., Li, W., et al., 1998. Late Cenozoic Xianshuihe/Xiaojiang and Red River Fault Systems of Southwestern Sichuan and Central Yunnan, China. Special Paper of the Geological Society of America 327. pp. 1–108. https://doi.org/10.1130/0-8137-2327-2.1.
Wang, S.F., Fang, X.M., Zheng, D.W., Wang, Erchie, 2009. Initiation of slip along the Xianshuihe Fault zone, estern Tibet, constrained by K/Ar and fission-track ages. Int. Geol. Rev. 51 (12), 1121–1131.
Wang, A., Qin, Y., Lan, F., 2013. Geochemical characteristics and microbial populations of Neogene brown coal from Zhaotong Basin, China. Environ. Earth Sci. 68 (6), 1539–1544. https://doi.org/10.1007/s12665-012-1847-0.
Winkler, A., Wolf-Welling, T., Stattegger, K., Thiede, J., 2002. Clay mineral sedimentation in high northern latitude deep-sea basins since the Middle Miocene (ODP Leg 151, NAAG). Int. J. Earth Sci. 91 (1), 133–148. https://doi.org/10.1007/s005310100199.
Xia, K., Su, T., Lie, Y.S., Xing, Y.W., Jacques, F.M.B., Zhou, Z.K., 2009. Quantitative climate reconstructions of the late Miocene Xiaolongtan megaflora from Yunnan, southwest China. Palaeogeogr. Palaeoclimatol. Palaeoecol. 276, 80–86. https://doi.org/10.1016/j.palaeo.2009.02.024.
Xing, Y.W., Utescher, T., Jacques, F.M.B., Su, T., Liu, Y.S., Huang, Y.J., Zhou, Z.K., 2012. Paleoclimatic estimation reveals a weak winter monsoon in southwestern China during the late Miocene: evidence from plant macrofossils. Palaeogeogr. Palaeoclimatol. Palaeoecol. 358-360, 19–26. https://doi.org/10.1016/j.palaeo.2012.07.011.
Xu, J.X., Ferguson, D.K., Li, C.S., Wang, Y.F., Du, N.Q., 2004. Climatic and ecological implications of Late Pliocene Palynoflora from Longling, Yunnan, China. Quat. Int. 117, 91–103. https://doi.org/10.1016/S1040-6182(03)00119-8.
Xu, J.X., Ferguson, D.K., Li, C.S., Wang, Y.F., 2008. Late Miocene vegetation and climate of the Lühe region in Yunnan, southwestern China. Rev. Palaeobot. Palynol. 148, 36–59. https://doi.org/10.1016/j.revpalbo.2007.08.004.
Xu, Q., Ding, L., Spicer, R.A., Liu, X., Li, S., Wang, H., 2017. Stable isotopes reveal southward growth of the Himalayan-Tibetan Plateau since the Paleocene. Gondwana Res. https://doi.org/10.1016/j.gr.2017.10.005.
Zachos, J., Pagani, M., Sloan, L., Thomas, E., Billups, K., 2001. Trends, rhythms, and aberrations in global climate 65 Ma to present. Science 292 (5517), 686–693. https://doi.org/10.1126/science.1059412.
Zhang, C., Guo, Z., 2014. Clay mineral changes across the Eocene–Oligocene transition in the sedimentary sequence at Xining occurred prior to global cooling. Palaeogeogr. Palaeoclimatol. Palaeoecol. 411, 18–29. https://doi.org/10.1016/j.palaeo.2014.06.031.
Zhang, P., Molnar, P., Downs, W.R., 2001. Increased sedimentation rates and grain size 2–4 Myr ago due to the influence of climate change on erosion rates. Nature 410 (19).
Zhang, Q.Q., Ferguson, D.K., Mosbrugger, V., Wang, Y.F., Li, C.S., 2012. Vegetation and climatic changes of SW China in response to the uplift of Tibetan Plateau. Palaeogeogr. Palaeoclimatol. Palaeoecol. 363-364, 23–36. https://doi.org/10.1016/j.palaeo.2012.08.009.
Zhang, C., Xiao, G., Guo, Z., Wu, H., Hao, Q., 2015a. Evidence of late early Miocene aridification intensification in the Xining Basin caused by the northeastern Tibetan Plateau uplift. Glob. Planet. Chang. 128, 31–46. https://doi.org/10.1016/j.gloplacha.2015.02.002.
Zhang, C., Paterson, G., Hu, B., Chang, L., Deng, C., Wu, H., Guo, Z., 2015b. Elevation Dependent Weathering and Padogenesis of the Emeishan Basalt in the Northeastern Yunnan, China. INQUA Conference Abstact T03-05. pp. T02409.
Zhang, C., Guo, Z., Deng, C., Ji, X., Wu, H., Paterson, G.A., Chang, L., Li, Q., Wu, B., Zhu, R., 2016. Clay mineralogy indicates a mildly warm and humid living environment for the Miocene hominoid from the Zhaotong Basin, Yunnan, China. Sci. Rep. 6, 20012. https://doi.org/10.1038/srep20012.
Zhao, L.C., Wang, Y.F., Liu, C.J., Li, C.S., 2004. Climatic implications of fruit and seed assemblage from Miocene of Yunnan, southwestern China. Quat. Int. 117, 81–89. https://doi.org/10.1016/S1040-6182(03)00118-6.
Zheng, H., Powell, C.M., Rea, D.K., Wang, J., Wang, P., 2004. Late Miocene and mid-Pliocene enhancement of the East Asian monsoon as viewed from the land and sea. Glob. Planet. Chang. 41 (3–4), 147–155. https://doi.org/10.1016/j.gloplacha.2004.01.003.
Zheng, Y.M., Zhong, W., Xue, J.B., Fan, X.P., Zeng, Z.G., Liu, W., et al., 2008. Sedimentary characteristics of dahu lacustrine-swamp at Dingnan, Jiangxi Province, Eastern Nanling mountains. Journal of South China Normal University 2, 129–135.
Zhuang, G.S., Pagani, M., Zhang, Y.G., 2017. Monsoonal upwelling in the western Arabian Sea since the middle Miocene. Geology 45 (7), 655–658. https://doi.org/10.1130/G39013.1.